Applied Catalysis B: Environmental 241 (2019) 329–337

Contents lists available at ScienceDirect

Applied Catalysis B: Environmental

journal homepage: www.elsevier.com/locate/apcatb

The selective deposition of MoS_2 nanosheets onto (101) facets of TiO_2 nanosheets with exposed (001) facets and their enhanced photocatalytic H_2 production

Xiaolin Hu, Shucao Lu, Jian Tian*, Na Wei, Xiaojie Song, Xinzhen Wang, Hongzhi Cui*

School of Materials Science and Engineering, Shandong University of Science and Technology, Qingdao 266590, China

ARTICLE INFO

Keywords:
Selective deposition
MoS_2 nanosheets
TiO_2 nanosheets
Exposed active facets
Photocatalytic H_2 production

ABSTRACT

One of the challenging issues in photocatalytic hydrogen (H_2) production is to efficiently separate the photogenerated electron-hole pairs and require the enrichment of photogenerated electrons on the photocatalyst's surface. Herein, a novel 2D-2D nanojunction of MoS_2 nanosheets (NSs) selectively deposited on the (101) facets of TiO_2 NSs with mainly exposed high-active (001) facets is prepared via a hydrothermal/annealing treatment combined with an photoreduction method using carbon fiber (CF) as templates. The obtained MoS_2@TiO_2 composite (selective deposition) photocatalyst exhibits a greatly enhanced photocatalytic H_2 production activity at the optimal weight percentage of MoS_2 (15 wt%), exceeding that of pure TiO_2 NSs and MoS_2@TiO_2 composites (random deposition) by 32 and 3 times, respectively. The superior photoactivity of MoS_2@TiO_2 composites (selective deposition) is attributed to the synergistic promoting effects of the following factors: (i) the mainly exposed (001) facets of TiO_2 NSs with higher surface energy in MoS_2@TiO_2 composites (selective deposition) facilitate the activation of water molecules and the photocatalytic reduction; (ii) the coexposed (101) and (001) facets can form a surface heterojunction within single TiO_2 NS, which is beneficial for the transfer and separation of charge carriers; (iii) the MoS_2 NSs are selectively deposited on the electrons-rich (101) facets of TiO_2 NSs, which can effectively reduce the charge carriers recombination rate by capturing photoelectrons. This study presents an inexpensive photocatalyst for energy conversion to achieve highly efficient H_2 evolution without noble metals.

1. Introduction

Solar energy has the advantages of being clean, abundant and renewable. Therefore, solar energy to hydrogen (H_2) energy conversion using photocatalytic water splitting is one of the promising methods to tackle serious energy and environmental problems [1]. Titanium dioxide (TiO_2) is one of the most important semiconductor-based photocatalysts and have been widely studied for photocatalytic H_2 production [2,3]. When TiO_2 is excited, both electron and hole are produced, and photocatalytic reactions happen when photogenerated electrons and holes migrate to its surface and react with substances absorbed on/near its surface [3]. However, the further application of TiO_2 is restricted due to the rapid recombination of photogenerated electron-hole pairs, thus numerous methods have been explored to solve this problem including doping and integrating narrow band gap semiconductors [4]. Since the pioneering report by Yang et al. in 2008 found that the 47% exposed (001) facets of anatase TiO_2 with high surface energies showed the highest photocatalytic activity [5], morphology engineering that can attain selectively exposed high-active crystal facets of TiO_2 is a promising approach to enhance the photocatalytic activity [6]. So far, TiO_2 with different exposed facets such as (001), (100) and (101) have been successfully obtained [7]. Theoretical calculations have demonstrated the order of the average surface energies of the main exposed crystal facets of the anatase TiO_2 crystals following: $0.90\ J/m^2$ for (001) $>$ $0.53\ J/m^2$ for (100) $>$ $0.44\ J/m^2$ for (101) [8]. Besides, anatase TiO_2 with exposed different crystal facets have also been widely developed to promote the transition of photogenerated charge carriers, because the (101) and (001) facets of anatase TiO_2 exhibit different band structures and band edge positions based on the density functional theory (DFT) calculation [9]. Thus, the exposed (101) and (001) facets can form a surface heterojunction, which is beneficial for the transfer of photogenerated electrons and holes to (101) and (001) facets, respectively, resulting in the enhancement of photocatalytic activity [10]. Moreover, co-catalysts, such as noble

* Corresponding authors.
E-mail addresses: jiantian@sdust.edu.cn (J. Tian), cuihongzhi1965@163.com (H. Cui).

https://doi.org/10.1016/j.apcatb.2018.09.051
Received 31 July 2018; Received in revised form 12 September 2018; Accepted 16 September 2018
Available online 17 September 2018
0926-3373/

metals (Au, Ag, Pt), deposited on the surface of TiO_2, can serve as trapping centers for photogenerated electrons and subsequently as active centers for photocatalytic H_2 production [11,12]. However, the use of noble metals for photocatalytic H_2 production from water may be difficult in practical applications due to their high-cost and scarcity [13]. Therefore, the quest for alternative low-cost cocatalysts to replace the noble metals materials is of utmost importance [14].

Molybdenum disulfide (MoS_2) is a typical two-dimensional (2D) layered transition metal sulfide with a structure composed of three stacked atom layers (S−Mo−S) [15]. The weak van der Waals bonding between these 2D layers often gives rise to single- or few-layer nanosheet (NS) architectures [16]. MoS_2 as a promising cost-effective substitute for noble metal cocatalysts shows superior photocatalytic H_2 evolution performance, owing that the unsaturated S atoms on the exposed edges of MoS_2 can act as active sites and have a strong affinity to H^+ in solution [17]. For instance, Lin et al. reported that integration of a certain quantity of MoS_2 NSs with CdS nanowires can effectively enhance the photocatalytic H_2 production [18]. In addition, as a 2D support, MoS_2 NSs can provide a platform for attaching other semiconductors to form 3D nanostructures, which favors photocatalytic H_2 evolution because they produce more reaction active sites than 1D and 2D nanostructured materials [19]. Therefore, 2D MoS_2 NSs can be combined with other semiconductors to form 3D nanostructures.

Both theoretical and experimental studies had demonstrated that (001) crystal facets are holes-rich and (101) crystal facets are electrons-rich in anatase TiO_2 [20]. Thus, the high-energy (001) facets prefer to provide oxidation sites, while the low-energy (101) facets prefer to provide reduction sites [21]. Traditionally, cocatalysts are loaded on semiconductors by a chemical precipitation or adsorption method, which, in most cases, results in a random distribution of the cocatalysts on the surface of the photocatalysts [22]. In this case, cocatalysts are possibly deposited on the wrong sites (e.g., the photocatalytic H_2 evolution cocatalyst, such as Pt, is deposited on the holes-rich (001) facets in anatase TiO_2), which leads to the increase of the recombination of charge carriers [23]. Thus, it would be desirable to selectively deposit MoS_2 NSs onto electrons-rich (101) facets of TiO_2 NSs, which could combine the advantages from both the crystal facet effect and cocatalyst modification to initiate the oriented migration of photogenerated electrons and further enrich their presence onto the surface of TiO_2 for the enhanced photocatalytic H_2 production activity. To the best of our knowledge, the selective deposition of MoS_2 NSs on well-defined TiO_2 nanocrystals and investigation of their shape-dependent photocatalytic performance in H_2 production are not yet reported in the open publications.

Herein, we for the first time fabricate novel and unique 2D MoS_2 NSs selectively deposited on the (101) facets of 2D TiO_2 NSs with mainly exposed high-active (001) facets using carbon fibers (CFs) as templates, via a hydrothermal/annealing treatment method and subsequent photoreduction method. The results demonstrate that this MoS_2@TiO_2 composites (selective deposition) exhibit higher activity in photocatalytic H_2 production than that of pure TiO_2 NSs and MoS_2@TiO_2 composites (random deposition) under solar light irradiation. In this case, the mainly high-active exposed (001) facets facilitate the activation of water molecules and the photocatalytic reduction. Besides, the photogenerated electrons and holes can be respectively transferred onto (101) and (001) facets due to the presence of surface heterojunction. Furthermore, the selective deposited of MoS_2 NSs can capture photogenerated electrons of (101) facets and act as reduction active sites, leading to high photocatalytic H_2 production activity. This work may provide a particular viewpoint for designing new photocatalyst systems for H_2 production.

2. Experimental section

2.1. Materials

The chemicals used in this work were of analytical reagent grade. Butyl titanate ($Ti(OBu)_4$), carbon fibers (CFs), hydrochloric acid (HCl), hydrofluoric acid (HF, 40%), ammonium molybdate ($(NH_4)_2MoS_4$), molybdenum dioxide (MoO_2), and sulfur powder were purchased from Sinopharm.

2.2. Synthesis of TiO_2 nanosheets (NSs)

In a typical synthesis process, 1.0 mL $Ti(OBu)_4$ and 0.3 g CFs were slowly dropped into HCl (18 mL, 5 M) solution. After the solution had been stirred for 30 min, 0.35 mL HF was added to the mixed solution. After another 5 min stirring, the solutions were transferred into Teflon-lined stainless-steel autoclaves with a total volume of 25 mL. The hydrothermal synthesis was conducted at 180 °C for 4 h in an electric oven. Then, the obtained CF@TiO_2 composites were ultrasonically cleaned for 3 min in water. The TiO_2 NSs were obtained by annealing the as-prepared CF@TiO_2 composites at 800 °C for 2 h to remove the CF templates.

2.3. Synthesis of MoS_2@TiO_2 composites (selective deposition and random deposition)

The formation process of MoS_2@TiO_2 composites (selective deposition) was described as follows. Typically, 16.3 mg $(NH_4)_2MoS_4$ was respectively dissolved in 20 mL deionized water to form a transparent solution. Then 90 mg TiO_2 NSs were added into the above solution and stirred to form the suspension. The suspension was bubbled with N_2 for 30 min to remove oxygen completely and then irradiated with a 300 W mercury lamp for 60 min. The MoS_4^{2-} was reduced into the loaded MoS_2 by the photoexcited electrons of TiO_2. The MoS_2@TiO_2 composites (selective deposition, 10 wt% MoS_2) were harvested after centrifugation and dried at 50 °C for 12 h. Similarity, by changing the mass of $(NH_4)_2MoS_4$ (25.8 mg, 62.7 mg, and 146.3 mg), MoS_2@TiO_2 composites (selective deposition) with other MoS_2 loading amounts (15 wt %, 30 wt%, 50 wt%) were obtained, respectively.

For the preparation of MoS_2@TiO_2 composites (random deposition) with 15 wt% MoS_2 loading amounts, certain weights of MoO_2 and TiO_2 NSs were dispersed into DI water and the solution was stirred at 60 °C for 12 h. After water evaporation, MoO_2 was deposited on the surface of whole TiO_2 NSs. Finally, MoO_2 was completely changed into MoS_2 in a quartz-tube furnace at 500 °C using sulfur powder as sulfur sources.

2.4. Characterization

X-ray powder diffraction (XRD) patterns were recorded with a Bruke D8 Advance powder X-ray diffractometer with Cu Kα (λ = 0.15406 nm). Scanning electron microscopy (SEM) was performed with a FEI NanoSEM 450 instrument with an energy-dispersive X-ray spectroscopy (EDS). High resolution transmission electron microscopy (HRTEM) images were carried out with a JOEL JEM 2100F microscope. X-ray photoelectron spectroscopy (XPS) was performed using an ESCALAB 250. The UV–vis diffuse reflectance spectra (DRS) were tested with a UV–vis spectrophotometer (UV-3101, Shimadzu). The specific surface area was calculated using the BET method and examined on a Micromeritics ASAP2020 instrument. The photoluminescence (PL) spectra were acquired at room temperature with a FLS920 fluorescence spectrometer under the ultraviolet excitation of 325 nm.

2.5. Photocatalytic and photoelectrochemical activity test

Photocatalytic H_2 evolution experiments were mainly carried out in a Pyrex glass cell with a top window connected to a gas-closed system.

The experiments were performed in aqueous acetone which dissolved sacrificial reagent (TEOA), and suspended with 20 mg of catalysts powder following ultrasonic dispersion for 20 min. The reaction temperature of reactant solution was maintained at 25 °C. The reactant solution was irradiated with a 300 W Xe arc lamp with an AM-1.5 filter after the reaction solution was evacuated several times to remove air completely. The focused intensity on the flask was ca. 180 mW/cm^2. The generated hydrogen analyzed using gas chromatography (Beijing China Education Au-light Co., Ltd, 7920, nitrogen as a carrier gas) equipped with thermal conductivity detector (TCD). The apparent quantum efficiency (AQE) was measured under similar photocatalytic reaction condition except that four 365 nm-LEDs (3 W, Shenzhen LAMPLIC Science Co. Ltd., China) were used as light sources instead of the Xe arc lamp. The focused intensity for each 365 nm-LED was ca. 6.0 mW/cm^2. The apparent quantum efficiency (QE) was measured and calculated according to Eq. (1):

$$\mathrm{AQE} = \frac{\text{number of reacted electrons}}{\text{number of incident photons}} \times 100 = \frac{\text{number of evolved } H_2 \text{ molecules} \times 2}{\text{number of incident photons}} \times 100\% \tag{1}$$

Transient photocurrent responses (PEC) and electrochemical impedance spectroscopy (EIS) curves were measured under a 300 W Xe arc lamp with an AM-1.5 filter with light on-off switches of 50 s in a three-electrode electrochemical cell in the 0.5 M Na_2SO_4 electrolyte, in which Pt foil and $Hg/Hg_2Cl_2/KCl$ (saturated) electrode were used as the counter and reference electrodes, respectively. 10 mg as-synthesized samples were mixed with 1 mL ethanol. After sonicated for 15 min, the mixture was dropped onto fluoride-tin oxide (FTO) conductor glass and dried at 60 °C for 2 h to form a working electrode.

3. Results and discussion

Titanium dioxide (TiO_2) is a typical semiconductor belonging to the anatase phase and has shown photocatalytic activity in H_2 production [24]. Morphology engineering that can attain selectively exposed high-active crystal facets is a promising approach to enhance the activity of photocatalysts [25]. Hence, the TiO_2 NS is chosen as an ideal model to achieve charge carriers separation and selective loading of cocatalysts as catalytic sites for photocatalytic H_2 production. The formation procedure for the MoS_2@TiO_2 composites (selective deposition) is shown in Scheme 1. First, the TiO_2 NSs (blue) with two different types of exposed facets, electrons-rich (101) crystal facets and holes-rich (001) facets, are first grown on the surface of the CF (black) using $Ti(OBu)_4$ as the precursor in a HF aqueous solution according to a previously reported method [26]. Second, CF@TiO_2 annealing at 800 °C for 2 h is to remove the CF templates, TiO_2 NSs with a regular morphology and smooth surface with coexposed (001) and (110) facets are obtained. Subsequently, photoreduction treatment of $(NH_4)_2MoS_4$ in an aqueous solution of the as-prepared TiO_2 NSs lead to ultrathin MoS_2 NSs (grey) selectively grown on the electrons-rich (101) facets of the TiO_2 NSs.

XRD was used to investigate the phase structure and crystallization of the prepared samples. Fig. 1 shows the XRD patterns of MoS_2@TiO_2 composites (selective deposition) with different MoS_2 loading amounts. As can be seen, no signals assignable to CFs are detectable. This indicates that the CFs disappear by annealing the CF@TiO_2 composites. Additionally, the curves reveal that the diffraction peaks at about 2θ = 25.28°, 36.95°, 37.80°, 38.58°, 48.05°, 53.89°, 55.06°, 62.69°, 68.76°, 70.31° and 82.66° correlate closely with the (101), (103), (004), (112), (200), (105), (211), (204), (116), (220) and (224) crystal planes of anatase TiO_2 (JCPDS card no. 21-1272) [3]. No signals assignable to MoS_2 are detectable. This can be explained by the fact that MoS_2 is ultra-thin and is high dispersed on the TiO_2 NSs, as shown in the TEM images of Fig. 3.

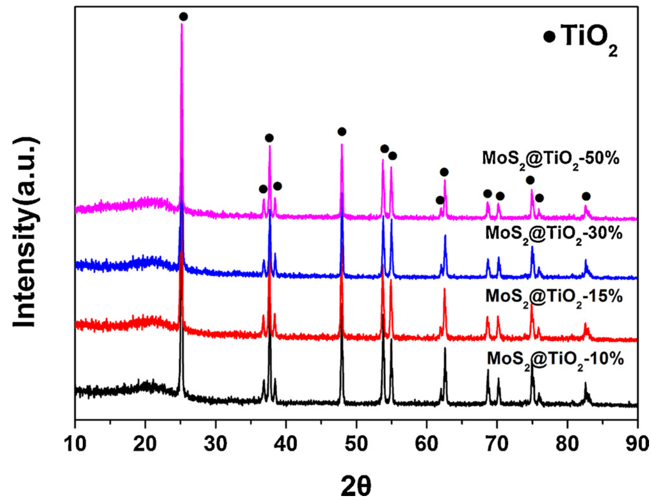

Fig. 1. XRD patterns of MoS_2@TiO_2 composites (selective deposition) with different MoS_2 loading amounts (10 wt%, 15 wt%, 30 wt%, 50 wt%).

Fig. 2a shows the SEM image of TiO_2 NSs, in which TiO_2 NS is a sheet shaped structure with an average side length of ca. 3 μm and thickness of ca. 200 nm. According to the symmetries of TiO_2 NSs, two flat and square surfacets in the crystal structure of TiO_2 NSs can be ascribed to (001) facets and the eight isosceles trapezoidal surfacets are (101) facets of the TiO_2 crystal. A magnified FE-SEM image (Fig. 2b) exhibits these two facets clearly, besides, it can be seen that the interfacial angle between the (001) and (101) facets of anatase is 68° on average [27]. From their size and geometry, the percentages of exposed facets in the as-prepared TiO_2 nanocrystals were calculated on TiO_2 nanocrystals by the method developed by Zhu et al. [28]. The average percentage of the exposed (001) facets was 56.8% (The method of the calculation is shown in Fig. S1). Note that this exposed percentage of (001) facets is very close to that reported recently (58%) for the optimized formation of a surface heterojunction [29]. As shown in Fig. 2c, interestingly, the MoS_2 NSs with a very thin layer mainly appeared on the (101) facets of TiO_2 NSs, while almost no MoS_2 NSs were observed on the (001) facets. This phenomenon was also confirmed by a magnified FE-SEM image of TiO_2 NSs (Fig. 2d), which can keep the maximum exposure of (001) facets of TiO_2 NSs with higher surface energy. Therefore, it can be concluded that MoS_2 NSs are selectively deposited on the (101) facets of TiO_2 NSs [30]. Moreover, MoS_2@TiO_2 composites (selective deposition) with other different MoS_2 loading amounts (10 wt %, 30 wt%, 50 wt%) are also obtained. The corresponding SEM images

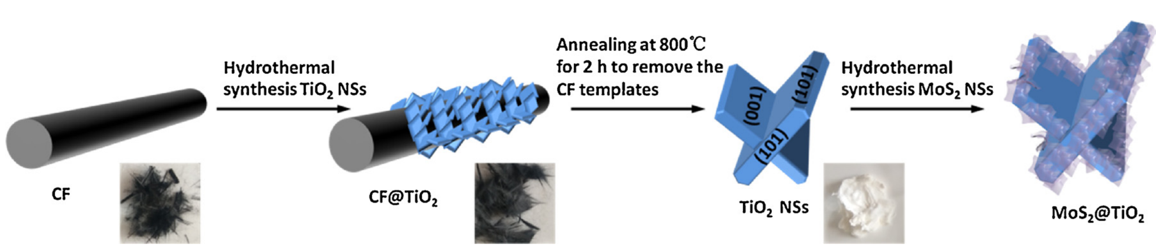

Scheme 1. Schematic illustration of the formation of the MoS_2@TiO_2 composites (selective deposition).

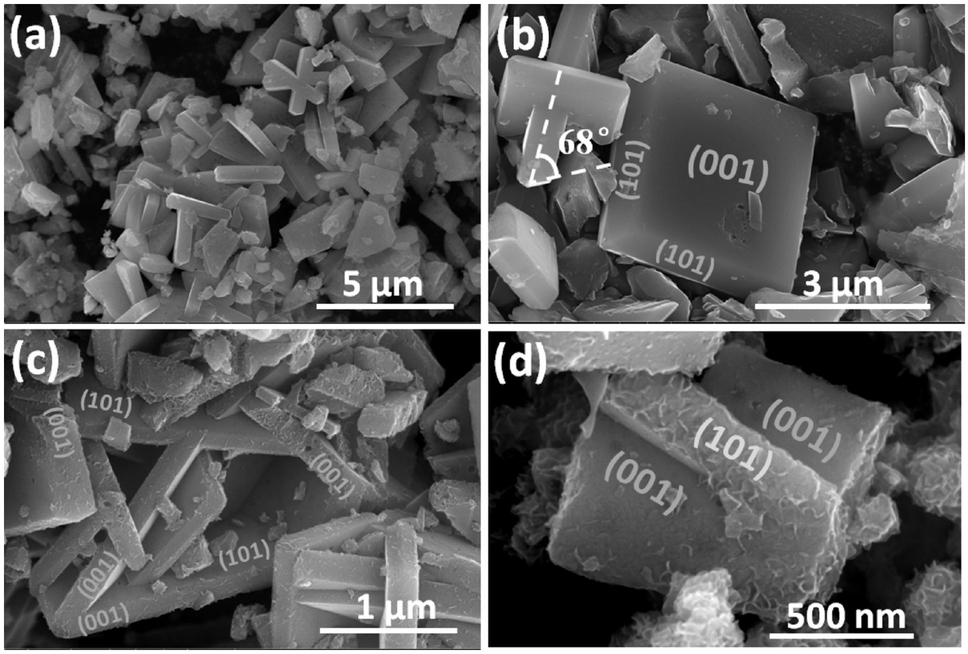

Fig. 2. SEM images of (a, b) TiO_2 NSs and (c, d) $MoS_2@TiO_2$ composites (selective deposition, 15 wt% MoS_2).

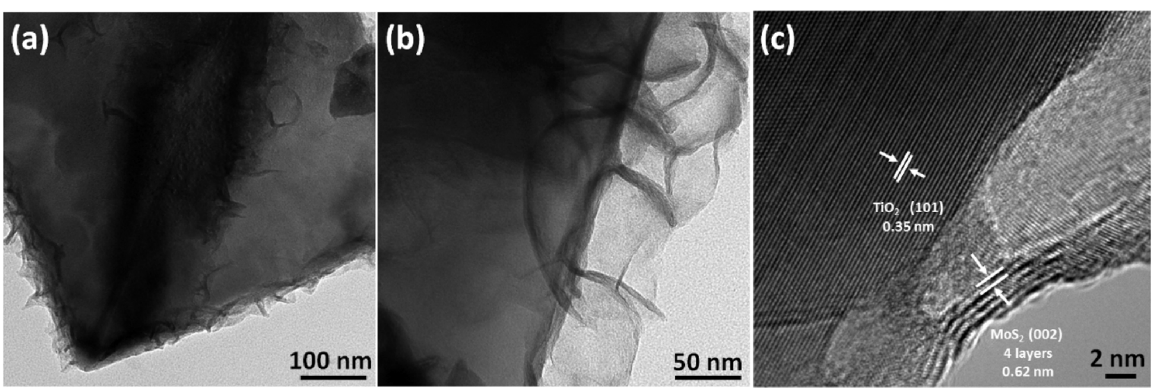

Fig. 3. TEM images of $MoS_2@TiO_2$ composites (selective deposition, 15 wt% MoS_2).

are presented in Fig. S2. EDS (Fig. S3 and Table S1) shows that Mo, S, Ti, and O elements are found in the $MoS_2@TiO_2$ composites (selective deposition), and no other impurities are observed in the spectra.

The morphologies of $MoS_2@TiO_2$ composites were further confirmed by transmission electron microscopy (TEM) observations (Fig. 3). As shown in the Fig. 3a and b, thin MoS_2 NSs are intimately deposited on the (101) facets of TiO_2 NSs with few layers. HR-TEM image of $MoS_2@TiO_2$ composite showed the intimate contact between MoS_2 and TiO_2 (Fig. 3c). The lattice spacing of ca. 0.62 nm can be assigned to the (002) plane of hexagonal MoS_2 (JCPDS, No.37-1492) [31], and the lattice spacing of ca. 0.35 nm can be indexed to the (101) plane of anatase TiO_2 (JCPDS, No. 21-1272) [32]. Based on the above analyses, it could be concluded that MoS_2 NSs are selectively deposited on the (101) facets of TiO_2 NSs. Moreover, the intimate contact between MoS_2 NSs and TiO_2 NSs in the 2D-2D $MoS_2@TiO_2$ composites could favor the transfer of photogenerated charge carriers, thus enhancing the charge separation and the photocatalytic activity [33].

X-ray photoelectron spectroscopy (XPS) was used to investigate the chemical states of Ti, O, Mo and S in the $MoS_2@TiO_2$ composites. The XPS survey spectrum (Fig. S4) indicates that $MoS_2@TiO_2$ composites are consisted of Ti, O, Mo, S and C elements without other impurities. Among them, the C element peak is mainly attributed to exogenous carbon as a calibration reference. The binding energies of Ti $2p_{3/2}$ and Ti $2p_{1/2}$ for $MoS_2@TiO_2$ composites are located at 459.3 and 465.3 eV (Fig. 4a), respectively, indicating the presence of Ti^{4+} [34]. The O 1s spectra of MoS2@TiO_2 composites is shown in Fig. 4b, in which two peaks with binding energies of 530.8 and 531.9 eV are observed, which are attributed to the Ti—O bond and adsorbed water, respectively [35]. Fig. 4c and d show that the binding energies of Mo $3d_{3/2}$, Mo $3d_{5/2}$, S $2p_{1/2}$ and S $2p_{3/2}$ peaks are located at 232.5, 229.3, 163.9 and 162.3 eV [36], respectively, suggesting that Mo^{4+} and S^{2-} existed in the $MoS_2@TiO_2$ composites. The states of Ti, O, Mo and S are all in agreement with TiO_2 and MoS_2, according to the XPS spectra.

The solar light harvesting of $MoS_2@TiO_2$ composites was investigated through UV–vis absorption spectra, as shown in Fig. 5a. MoS_2 NSs exhibit a remarkable absorption in the visible region (400–800 nm). Compared to the pure TiO_2 NSs, the absorption spectra of the $MoS_2@TiO_2$ composites show an enhanced absorption in the visible light region ranging from 400 to 800 nm, and increases with the increasing MoS_2 content, which is in accordance with the above color change of the sample from white to black (Fig. S5). The band gap energy (E_g) of TiO_2 NSs, MoS_2 NSs and $MoS_2@TiO_2$ composites with different MoS_2 loading amounts (10 wt%, 15 wt%, 30 wt% and 50 wt% MoS_2) could be computed from the formula $(\alpha h\nu)^{1/2} \propto h\nu - E_g$, where α, h, ν, and E_g are absorption coefficient, Planck's constant, light frequency, and band gap energy, respectively (Fig. 5b). Thus, after

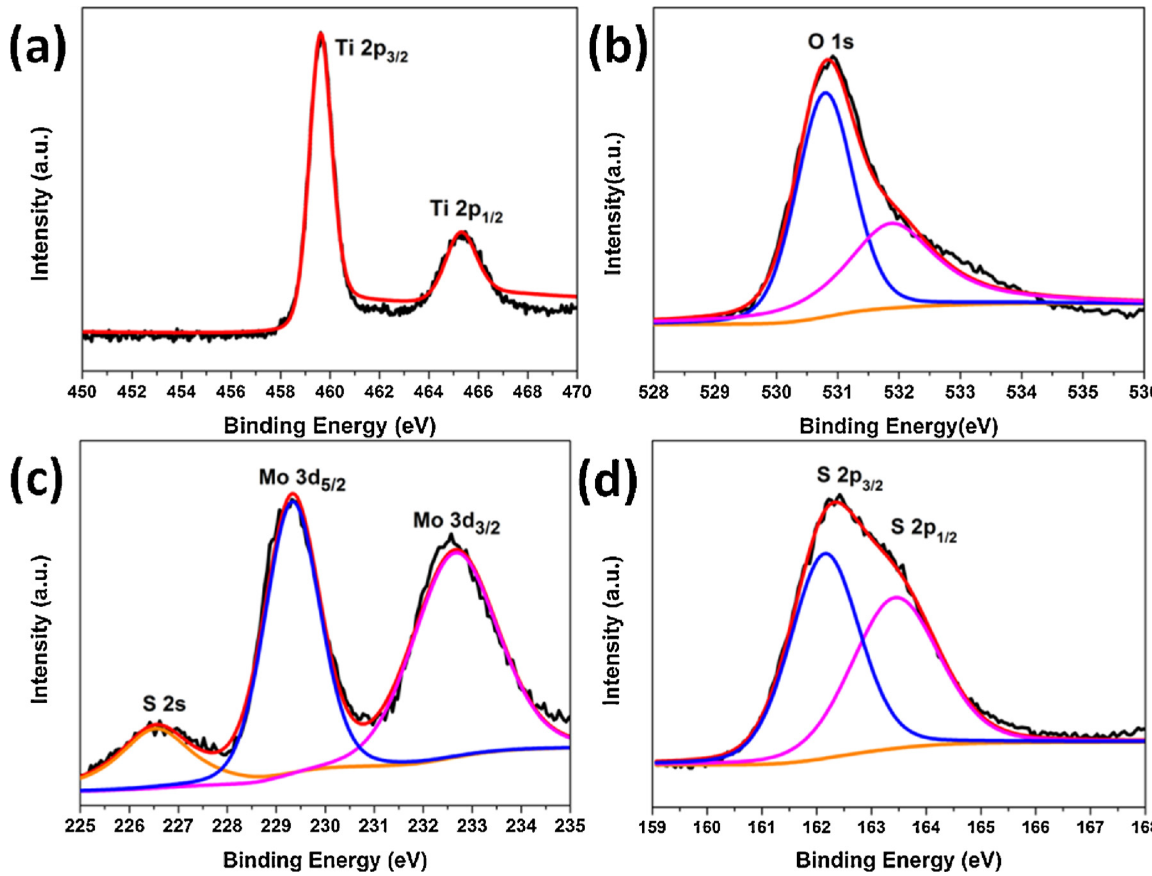

Fig. 4. XPS spectra of (a) Ti 2p, (b) O 1s, (c) Mo 3d and (d) S 2p in $MoS_2@TiO_2$ composites (selective deposition, 15 wt% MoS_2).

calculating, the E_g of TiO_2 NSs, MoS_2 NSs and $MoS_2@TiO_2$ composites with different MoS_2 loading amounts (10 wt%, 15 wt%, 30 wt% and 50 wt% MoS_2) are found to be about 3.1 eV, 0.6 eV, 1.32 eV, 1.23 eV, 1.13 eV and 0.84 eV, separately. Besides, the absorption spectra of the $MoS_2@TiO_2$ composites show a red-shift of absorption edge with increasing MoS_2 contents (Fig. 5a), due to the narrow band gap of MoS_2 (0.6 eV, Fig. 5b). This result indicates that the addition of MoS_2 can enhance the optical absorption properties.

The photocatalytic activity for H_2 evolution was evaluated under simulated sunlight irradiation using acetone as a scavenger. Fig. 6 presents a comparison of the photocatalytic H_2 production activities of TiO_2 NSs, MoS_2 NSs and $MoS_2@TiO_2$ composites (selective deposition, 10 wt%, 15 wt%, 30 wt% and 50 wt% MoS_2) in aqueous acetone solution with TEOA to quench the photogenerated holes. Control experiments (Fig. S6) indicate that no appreciable H_2 production is detected in the absence of either irradiation or photocatalyst, suggesting that H_2 is produced by a photocatalytic reaction of the photocatalyst. Pure MoS_2 NSs and TiO_2 NSs are photocatalytically inert toward H_2 production, with a reaction rate of lower than 0.06 mmol g^{-1} h^{-1} (Fig. 6a). The low photocatalytic H_2 production of pure MoS_2 is probably due to the number of photogenerated electron and holes in the MoS_2 band structure not being sufficient to produce a detectable amount of H_2 [37]. Pure TiO_2 shows a very low photocatalytic activity because of the rapid recombination of electrons and holes [38]. Noticeably, as shown

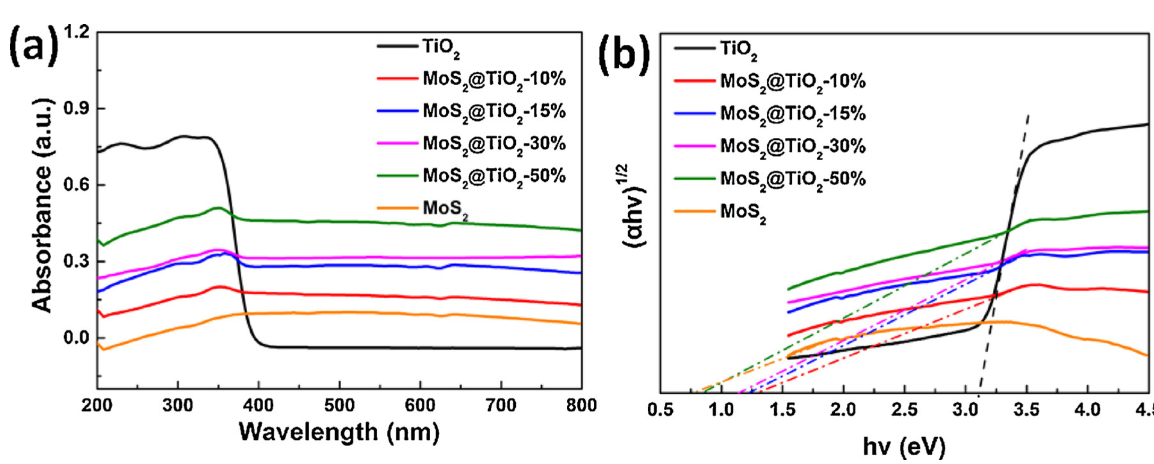

Fig. 5. (a) UV–vis absorption spectra and (b) band gap values of TiO_2 NSs, MoS_2 NSs and $MoS_2@TiO_2$ composites (selective deposition) with different MoS_2 loading amounts (10 wt%, 15 wt%, 30 wt% and 50 wt% MoS_2).

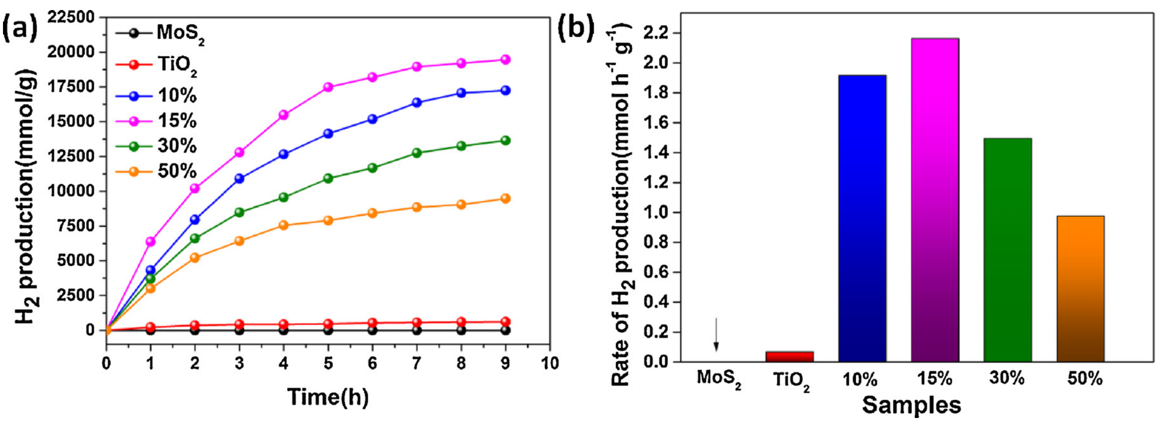

Fig. 6. (a) Photocatalytic H_2 production and (b) rate of photocatalytic H_2 production of different catalysts in aqueous acetone solution with TEOA within 9 h.

in Fig. 6a the photocatalytic activity is sharply enhanced with MoS_2 loading and achieves maximal values on the MoS_2@TiO_2 composites (15 wt% MoS_2), reaching 2.16 mmol g^{-1} h^{-1} (32 times that of pure TiO_2). The superior photocatalytic H_2 production of the MoS_2@TiO_2 composites suggest that MoS_2 modification on TiO_2 is critical to the photocatalytic H_2 production. As an effective water reduction cocatalyst, MoS_2 has been widely used as cocatalyst for enhancing photocatalytic H_2 production [39]. The deposition of MoS_2 NSs acted as the electron sinks to facilitate the separation of photoelectrons from holes, thus leading to an enhanced H_2 production activity [40].

In addition, as shown in Fig. 6b, the photocatalytic activities of the samples increase non-linearly with increasing MoS_2 loading (from 10 to 15 wt% MoS_2) because of the relatively lower solar energy input via increasing catalyst amount. However, further increasing the content of MoS_2 (from 15 wt% to 50 wt% MoS_2) leads to a gradual decrease of the photocatalytic activity. Excess black MoS_2 NSs absorb photons in the photocatalytic system, probably decreasing the intensity of light through the deeper reaction solution and shielding the light from reaching the TiO_2 surface, which could be called a "shielding effect" [41]. This shielding effect may become more obvious and then gradually decrease the photocatalytic activity when further increasing the MoS_2 content, which is consistent with the change of the sample color (Fig. S5) and the UV–vis spectra (Fig. 5a). Stability and recyclability of the MoS_2@TiO_2 composites (selective deposition) were estimated by repeating intermittent H_2 evolution under solar light (Fig. S7). 90% of incipient production can be kept for the MoS_2@TiO_2 composites even after 20 h. Besides, the rate of H_2 evolution of the MoS_2@TiO_2 composites within 20 h after 3 cycles keep seems to be linear (Fig. S8), which is better than that of in initial cycle (Fig. 6a). XRD pattern, SEM image and XPS spectra of MoS_2@TiO_2 composites (selective deposition, 15 wt% MoS_2) after 3 cycles in Fig. S9 show no obvious difference between those of the fresh sample. It further demonstrates the stability of the MoS_2@TiO_2 composites. Moreover, it is obvious that MoS_2@TiO_2 composites (15 wt% MoS_2) possess a larger BET surface area (Table S2) than that of TiO_2 NSs, MoS_2 NSs and MoS_2@TiO_2 composites with other MoS_2 loading amounts (10 wt%, 30 wt% and 50 wt% MoS_2), which is beneficial for the adsorption and migration of reactant and product molecules.

In order to further investigate the influence of the distribution of MoS_2 cocatalysts on the photocatalytic H_2 production activity of the prepared composites, the MoS_2 is deposited selectively and randomly on the TiO_2 NSs for comparison (Fig. 7). For sample MoS_2@TiO_2 composites (selective deposition), MoS_2 is selectively deposited on (101) facets of TiO_2 by photoreduction method. Similarly, for sample MoS_2/TiO_2 composites (random deposition), MoS_2 is randomly deposited on (101) and (001) facets of TiO_2 by sulfuration method. The selective and random deposition procedures of MoS_2 are illustrated in Figs. S10 and S11. During the selective photodeposition of MoS_2 cocatalyst (Fig. S10), due to the surface heterojunction between the two exposed facets, the photogenerated electrons and holes migrate to (101) and (001) facets, respectively. Consequently, Mo^{6+} in $(NH_4)_2MoS_4$ can be reduced effectively by the electrons on the (101) facets to form Mo^{4+}, which then further form MoS_2. The MoS_2 NSs are finally deposited on the (101) facets of TiO_2. Hence, the surface MoS_2 cocatalyst can be selectively deposited on (101) facets as the reduction active site, and the photogenerated electrons from TiO_2 are most likely to migrate to these reduction active sites to participate in photocatalytic H_2 production. However, for MoS_2@TiO_2 composites (random deposition) (Fig. S11), we chose MoO_2 (Mo^{4+}) as precursor because there is no reduction process. Certain weights of MoO_2 and TiO_2 are dispersed into DI water and the solution is stirred at 60 °C for 12 h. After water evaporation, MoO_2 is deposited on the surface of whole TiO_2 NSs. Finally, MoO_2 is completely changed into MoS_2 in a quartz-tube furnace using sulfur powder as sulfur sources. Thus, these MoS_2 NSs were randomly attached on (101) and (001) facets of TiO_2 NSs (Fig. S12). Therefore, it is not surprising that the photocatalytic activities of MoS_2@TiO_2 composites (random deposition) greatly decrease comparing with MoS_2@TiO_2 composites (selective deposition) because MoS_2 NSs are selectively deposited on (101) facets and used as reduction cocatalysts (Fig. 7). The random deposition of catalysts can lead to the reduction cocatalyst (MoS_2) being located on the wrong sites (oxidation sites) so that the recombination of photogenerated charge carriers can take place once they are trapped by the cocatalysts. To determine the photogenerated charge separation efficiency on the two types of MoS_2@TiO_2 composites, apparent quantum efficiency (AQE) was measured under light irradiation 365 nm. The AQE of water reduction for the MoS_2@TiO_2 composite (selective deposition) was measured to be about 3 times that of MoS_2@TiO_2 composite (random deposition), from 2.42% to 6.87%, demonstrating that charge separation efficiency is greatly improved by depositing MoS_2 NSs on (101) facets of TiO_2 NSs.

In order to further evaluate the efficiency of charge carrier trapping, migration, transfer, and separation, the photocurrent responses and electrochemical impedance spectroscopy of the samples were tested. Figs. 8a and S13 shows the periodic on/off photocurrent response of all samples when irradiated under solar light. It can be seen that all the samples show an immediate rise in the photocurrent response when the light was on. Contrarily, the photocurrent rapidly decreases to zero when the light was turned off. The on-off cycles of photocurrent are reproducible, which indicates that the photogenerated electrons are transferred to the back contact across the samples to form photocurrent under light irradiation [7]. The pure TiO_2 and MoS_2 electrode generated a relatively low photocurrent density with a 0.12 μA/cm^2 and 0.1 μA/cm^2, respectively. The MoS_2@TiO_2 composite (selective deposition, 15 wt%) electrode shows the highest photocurrent density of 1.3 μA/cm^2, which is about 11 times higher than that of bare TiO_2 electrode, indicating a noticeable improvement of electron-hole

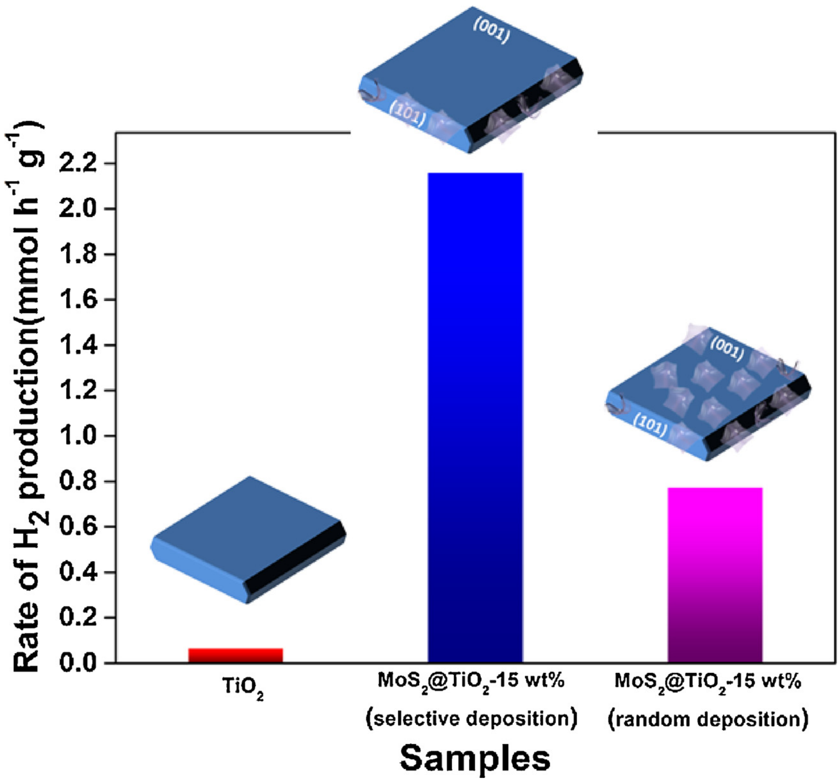

Fig. 7. (a) Rate of photocatalytic H_2 production of TiO_2 NSs, MoS_2@TiO_2 composite (selective deposition) and MoS_2@TiO_2 composite (random deposition).

separation efficiency by the introduction of MoS_2 cocatalysts [42]. The MoS_2@TiO_2 composite (50 wt%) electrode is only slight higher than bare TiO_2 electrode, due to modification of TiO_2 NSs with too much black MoS_2 NSs induced "shielding effect". Meanwhile, the excessive MoS_2 NSs on TiO_2 can act as a kind of recombination center instead of providing an electron pathway [43]. In general, a smaller arc radius on an EIS Nyquist plot means a smaller charge-transfer resistance on the electrode surface and a higher separation efficiency of electron-hole pairs. As shown in Fig. 8b, the arc size for the samples under solar light irradiation are MoS_2@TiO_2-15% < MoS_2@TiO_2-10% < MoS_2@TiO_2-30% < MoS_2@TiO_2-50% < TiO_2, suggesting that the MoS_2@TiO_2 composite (15 wt%) owns the most effective separation of photogenerated charges. The photoluminescence (PL) spectra (Fig. S14) can also confirm the MoS_2@TiO_2 composite (15 wt%) can effectively diminish the recombination of photogenerated carriers.

From what has been observed and discussed above, a proposed mechanism for the enhanced photocatalytic H_2 production activities of MoS_2@TiO_2 composites is illustrated in Scheme 2. For sample MoS_2@TiO_2 composites (selective deposition), under light illumination, the photoexcited electrons and holes are generated in the conduction band (CB) and valance band (VB) of TiO_2, respectively. Based on the DFT calculations, the (101) and (001) facets of anatase TiO_2 exhibit diff ;erent band structures and band edge positions [44]. Thus, the coexposed (101) and (001) facets of anatase can form a surface heterojunction within single TiO_2. Due to the presence of surface heterojunction, the photogenerated electrons and holes migrate to (101) and (001) facets, respectively [45,9]. On the (101) facets, the photoexcited electrons then transport to MoS_2 due that MoS_2 NSs contain several individual sandwiched S—Mo—S layers via weak van der Waals interactions, which lead to the abundant exposure of Mo-terminated edges with the metallic character and a high d-electron density [3]. During the H_2 production in solution, the excited electrons in TiO_2 transfer to Mo sites with d-electron density. Then MoS_2 NSs act as the reduction active sites, in which the electrons can reduce H_2O to produce H_2 [7].

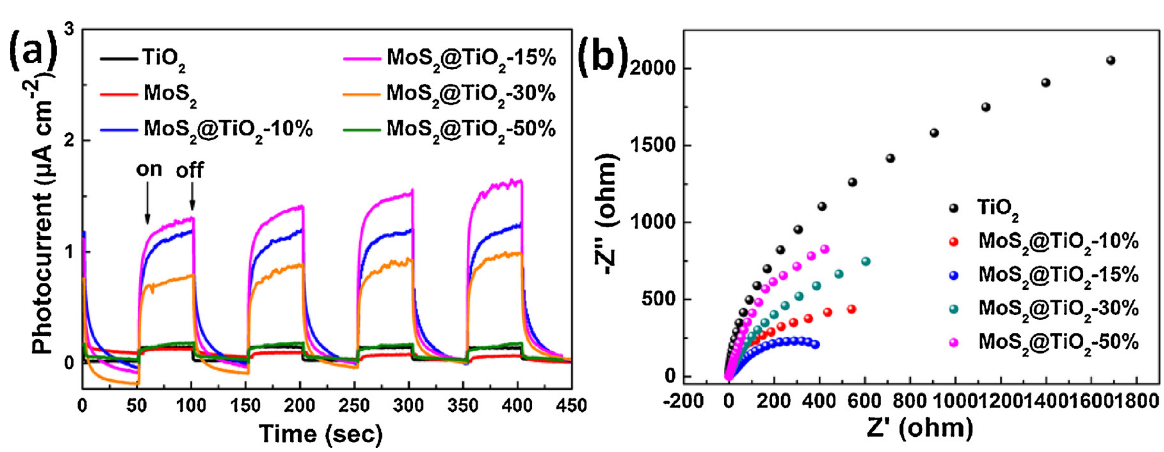

Fig. 8. (a) Transient photocurrent responses and (b) electrochemical impedance spectroscopy of the samples under solar light irradiation.

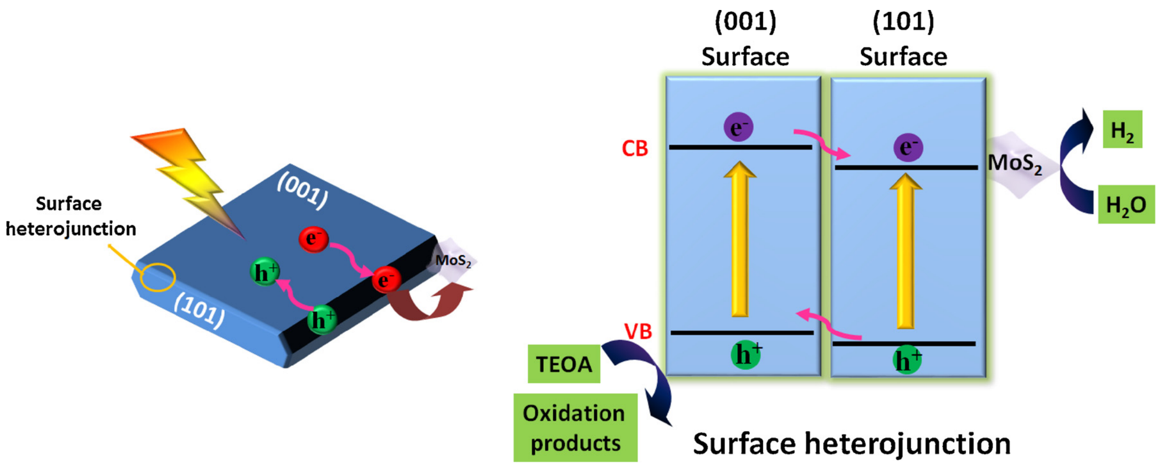

Scheme 2. Schematic illustration for the synergetic effect of the surface heterojunction between (101) and (001) facets and the selective deposition of MoS_2 on (101) facets of TiO_2. The former is beneficial for the spatial transfer and separation of photogenerated charged carriers and the latter beneficial for occurrence of reduction reactions.

The holes in (001) facets are consumed by the sacrificial reagents. This indicates that the notable synergetic effect was caused by the surface heterojunction and the cocatalysts.

However, for sample MoS_2@TiO_2 composites (random deposition), MoS_2 NSs were randomly loaded on both (101) and (001) facets. As a result, the MoS_2 NSs loaded on (001) facets will directly contact with holes on (001) facets, thus inhibiting the transfer of electrons from (001) to (101) facets, and becoming a recombination center of photogenerated electrons and holes. Therefore, it is easy to understand that the MoS_2@TiO_2 composite (random deposition) shows a lower H_2 production activity than MoS_2@TiO_2 composite (selective deposition). These results clearly show that not only the suitable contents of MoS_2 but also the loading locations of the cocatalysts are crucial for improving the photocatalytic H_2 production activity of TiO_2.

4. Conclusion

In summary, we have successfully developed an efficient MoS_2@TiO_2 composite photocatalyst with noble metal free MoS_2 NSs selectively deposited on the (101) facets of TiO_2 NS with mainly exposed high-active (001) facets by combining heterojunction nanostructure construction and morphology engineering method. The obtained MoS_2@TiO_2 composites (selective deposition) exhibits high photocatalytic H_2 evolution activity with a rate as high as 2.16 mmol $h^{-1}g^{-1}$, for the sample with 15 wt% MoS_2 loading, 32 and 3 times higher than pure TiO_2 NSs and MoS_2@TiO_2 composites (random deposition), respectively. For MoS_2@TiO_2 composites (selective deposition), the synergistic effect of surface heterojunction between (001) and (101) facets of TiO_2 NSs and the selective deposition of MoS_2 NSs on (101) facets largely suppress the recombination of charge carriers and provide more catalytic active sites for photocatalytic reactions and thus the photocatalytic activity is dramatically enhanced. The MoS_2@TiO_2 composite (selective deposition) photocatalyst also shows good stability under the reaction condition. The results show that not only the combination of MoS_2 cocatalysts but also the loading locations and distributions of the cocatalysts are very crucial for the enhancement of high photocatalytic H_2 production activity. Hopefully, the present results can provide useful information for designing optimal photocatalytic systems for H_2 production.

Acknowledgments

The authors are thankful for fundings from the National Natural Science Foundation of China (No. 51872173), Natural Science Foundation of Shandong Province (No. ZR2017JL020), Taishan Scholarship of Climbing Plan (No. tspd20161006), and Key Research and Development Program of Shandong Province (No. 2018GGX102028).

Appendix A. Supplementary data

Supplementary material related to this article can be found, in the online version, at doi:https://doi.org/10.1016/j.apcatb.2018.09.051.

References

[1] D. Lang, T. Shen, Q. Xiang, ChemCatChem 7 (2015) 943–951.
[2] T. Kamegawa, K. Irikawa, H. Yamashita, Sci. Rep. 7 (2017) 13628.
[3] H. Yang, J. Tian, Y. Bo, Y. Zhou, X. Wang, H. Cui, J. Colloid Interface Sci. 487 (2017) 258–265.
[4] H. Tian, K. Shen, X. Hu, L. Qiao, W. Zheng, J. Alloys Comp. 691 (2017) 369–377.
[5] H.G. Yang, C.H. Sun, S.Z. Qiao, J. Zou, G. Liu, S.C. Smith, H.M. Cheng, G.Q. Lu, Nature 453 (2008) 638–641.
[6] W.-S. Wang, D.-H. Wang, W.-G. Qu, L.-Q. Lu, A.-W. Xu, J. Phys. Chem. C 116 (2012) 19893–19901.
[7] A. Meng, J. Zhang, D. Xu, B. Cheng, J. Yu, Appl. Catal. B: Environ. 198 (2016) 286–294.
[8] Q. Xiang, J. Yu, Chin. J. Catal. 32 (2011) 525–531.
[9] J. Yu, J. Low, W. Xiao, P. Zhou, M. Jaroniec, J. Am. Chem. Soc. 136 (2014) 8839–8842.
[10] X.-Q. Gong, A. Selloni, J. Phys. Chem. B 109 (2005) 19560–19562.
[11] M.A. Khan, M. Al-Oufi, A. Tossef, Y. Al-Salik, H. Idriss, Catal. Struct. React. 1 (2016) 192–200.
[12] U. Caudillo-Flores, M.J. Muñoz-Batista, M. Fernández-García, A. Kubacka, Appl. Catal. B: Environ. 238 (2018) 533–545.
[13] Y. Zhao, X. Jia, G.I.N. Waterhouse, L.-Z. Wu, C.-H. Tung, D. O'Hare, T. Zhang, Adv. Energy Mater. 6 (2016) 1501974.
[14] X. Yang, H. Huang, B. Jin, J. Luo, X. Zhou, RSC Adv. 6 (2016) 107075–107080.
[15] X. Zhang, Y. Guo, J. Tian, B. Sun, Z. Liang, X. Xu, H. Cui, Appl. Catal. B: Environ. 232 (2018) 355–364.
[16] N. Qin, J. Xiong, R. Liang, Liu Y, S. Zhang, Y. Li, Z. Li, L. Wu, Appl. Catal. B: Environ. 202 (2017) 374–380.
[17] X. Li, W. Li, M. Li, P. Cui, D. Chen, T. Gengenbach, L. Chu, H. Liu, G. Song, J. Mater. Chem. A 3 (2015) 2762–2769.
[18] H. Lin, Y. Li, H. Li, X. Wang, Nano Res. 10 (2017) 1377–1392.
[19] S.Y. Jeong, H.-M. Shin, Y.-R. Jo, Y.J. Kim, S. Kim, W.-J. Lee, G.J. Lee, J. Song, B.J. Moon, S. Seo, H. An, S.H. Lee, Y.M. Song, B.-J. Kim, M.-H. Yoon, S. Lee, J. Phys. Chem. 122 (2018) 7088–7093.
[20] J. Tian, X. Hu, H. Yang, Y. Zhou, H. Cui, H. Liu, Appl. Surf. Sci. 360 (2016) 738–743.
[21] Y. Cui, Q. Ma, X. Deng, Q. Meng, X. Cheng, M. Xie, X. Li, Q. Cheng, H. Liu, Appl. Catal. B: Environ. 206 (2017) 136–145.
[22] Q. Xu, B. Cheng, J. Yu, G. Liu, Carbon 118 (2017) 241–249.
[23] Z. Lian, W. Wang, G. Li, F. Tian, K.S. Schanze, H. Li, ACS Appl. Mater. Interfaces 9 (2017) 16959–16966.
[24] A.L. Luna, E. Novoseltceva, E. Louarn, P. Beaunier, E. Kowalska, B. Ohtani, M.A. Valenzuela, H. Remita, C. Colbeau-Justin, Appl. Catal. B: Environ. 191 (2016) 18–28.
[25] M.-V. Sofianou, V. Psycharis, N. Boukos, T. Vaimakis, J. Yu, R. Dillert, D. Bahnemann, C. Trapalis, Appl. Catal. B: Environ. 142–143 (2013) 761–768.

[26] W. Guo, F. Zhang, C. Lin, Z.L. Wang, Adv. Mater. 24 (2012) 4761–4764.
[27] H.G. Yang, G. Liu, S.Z. Qiao, C.H. Sun, Y.G. Jin, S.C. Smith, J. Zou, H.M. Cheng, G.Q. Lu, J. Am. Chem. Soc. 131 (2009) 4078–4083.
[28] J. Zhu, S. Wang, Z. Bian, S. Xie, C. Cai, J. Wang, H. Yang, H. Li, CrystEngComm 12 (2010) 2219.
[29] M.S. Akple, J. Low, Z. Qin, S. Wageh, A.A. Al-Ghamdi, J. Yu, S. Liu, Chin. J. Catal. 36 (2015) 2127–2134.
[30] C. Li, P. Zhang, R. Lv, J. Lu, T. Wang, S. Wang, H. Wang, J. Gong, Small 9 (2013) 3951–3956.
[31] H. Tian, M. Liu, W. Zheng, Appl. Catal. B: Environ. 225 (2018) 468–476.
[32] X. Hu, Y. Li, J. Tian, H. Yang, H. Cui, J. Ind. Eng. Chem. 45 (2017) 189–196.
[33] B. Chen, E. Liu, F. He, C. Shi, C. He, J. Li, N. Zhao, Nano Energy 26 (2016) 541–549.
[34] L. Zheng, S. Han, H. Liu, P. Yu, X. Fang, Small 12 (2016) 1527–1536.
[35] C. Liu, L. Wang, Y. Tang, S. Luo, Y. Liu, S. Zhang, Y. Zeng, Y. Xu, Appl. Catal. B: Environ. 164 (2015) 1–9.
[36] W. Zhou, Z. Yin, Y. Du, X. Huang, Z. Zeng, Z. Fan, H. Liu, J. Wang, H. Zhang, Small 9 (2013) 140–147.
[37] Q. Xiang, J. Yu, M. Jaroniec, J. Am. Chem. Soc. 134 (2012) 6575–6578.
[38] J. Tian, P. Hao, N. Wei, H. Cui, H. Liu, ACS Catal. 5 (2015) 4530–4536.
[39] Y. Zhu, Q. Ling, Y. Liu, H. Wang, Y. Zhu, Phys. Chem. Chem. Phys. 17 (2015) 933–940.
[40] Q. Liu, Z. Pu, A.M. Asiri, A.H. Qusti, A.O. Al-Youbi, X. Sun, J. Nanopart. Res. 15 (2013).
[41] H.-E. Kim, J. Lee, H. Lee, C. Lee, Appl. Catal. B: Environ. 115–116 (2012) 219–224.
[42] J. Zhuang, S. Weng, W. Dai, P. Liu, Q. Liu, J. Phys. Chem. C 116 (2012) 25354–25361.
[43] M. Ahmad, E. Ahmed, Z.L. Hong, J.F. Xu, N.R. Khalid, A. Elhissi, W. Ahmed, Appl. Surf. Sci. 274 (2013) 273–281.
[44] S. Liu, J. Yu, M. Jaroniec, Chem. Mater. 23 (2011) 4085–4093.
[45] Z. Zheng, B. Huang, J. Lu, X. Qin, X. Zhang, Y. Dai, Chemistry 17 (2011) 15032–15038.